Sympathoexcitation by hypothalamic paraventricular nucleus neurons projecting to the rostral ventrolateral medulla

Satoshi Koba[1] [iD], Eri Hanai[1], Nao Kumada[1], Naoya Kataoka[2], Kazuhiro Nakamura[2,3] [iD] and Tatsuo Watanabe[1]

[1] *Division of Integrative Physiology, Tottori University Faculty of Medicine, 86 Nishi-cho, Yonago, Tottori 683-8503, Japan*
[2] *Department of Integrative Physiology, Nagoya University Graduate School of Medicine, 65 Tsurumai-cho, Showa-ku, Nagoya 466-8550, Japan*
[3] *PRESTO, Japan Science and Technology Agency, 4-1-8 Honcho, Kawaguchi, Saitama 332-0012, Japan*

Edited by: Harold Schultz & Julie Chan

The Journal of Physiology

Key points

- Causal relationships between central cardiovascular pathways and sympathetic vasomotor tone have not been evidenced.
- This study aimed to verify the sympathoexcitatory role of hypothalamic paraventricular nucleus neurons that project to the rostral ventrolateral medulla (PVN-RVLM neurons).
- By using optogenetic techniques, we demonstrated that stimulation of PVN-RVLM glutamatergic neurons increased renal sympathetic nerve activity and arterial pressure via, at least in part, stimulation of RVLM C1 neurons in rats.
- This monosynaptic pathway may function in acute sympathetic adjustments to stressors and/or be a component of chronic sympathetic hyperactivity in pathological conditions such as heart failure.

Abstract The rostral ventrolateral medulla (RVLM), which is known to play an important role in regulating sympathetic vasomotor tone, receives axonal projections from the hypothalamic paraventricular nucleus (PVN). However, no studies have proved that excitation of the PVN neurons that send axonal projections to the RVLM (PVN-RVLM neurons) causes sympathoexcitation. This study aimed to directly examine the sympathoexcitatory role of PVN-RVLM neurons. Male rats received microinjections into the PVN with an adeno-associated virus (AAV) vector that encoded a hybrid of channelrhodopsin-2/1 with the reporter tdTomato (ChIEF-tdTomato), or into the RVLM with a retrograde AAV vector that encoded a channelrhodopsin with green fluorescent protein (ChR2-GFP$_{retro}$). Under anaesthesia with urethane and α-chloralose, photostimulation (473 nm wavelength) of PVN-RVLM neurons, achieved by laser illumination of either RVLM of ChIEF-tdTomato rats ($n = 8$) or PVN of ChR2-GFP$_{retro}$ rats ($n = 4$), elicited significant renal sympathoexcitation. Immunofluorescence confocal microscopy showed that RVLM adrenergic C1 neurons of ChIEF-tdTomato rats were
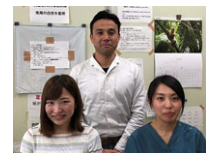
closely associated with tdTomato-labelled, PVN-derived axons that contained vesicular glutamate transporter 2. In another subset of anaesthetized ChIEF-tdTomato rats ($n = 6$), the renal sympathoexcitation elicited by photostimulation of the PVN was suppressed by administering ionotropic glutamate receptor blockers into the RVLM. These results demonstrate that excitation of PVN-RVLM glutamatergic neurons leads to sympathoexcitation via, at least in part, stimulation of RVLM C1 neurons.

Corresponding author S. Koba: Division of Integrative Physiology, Tottori University Faculty of Medicine, 86 Nishi-cho, Yonago, Tottori 683-8503, Japan.   Email: skoba@tottori-u.ac.jp

Introduction

The rostral ventrolateral medulla (RVLM) plays a pivotal role in the regulation of sympathetic vasomotor tone. This area contains spinally projecting, sympathetic premotor neurons, more than half of which are adrenergic C1 cells in rats (Jansen *et al.* 1995; Nam & Kerman, 2016). Selective stimulation of rat RVLM C1 neurons with optogenetic techniques elicits sympathoexcitation (Abbott *et al.* 2009). In addition, spinally projecting RVLM non-C1 cells, which lack enzymes for catecholamine biosynthesis, also regulate sympathetic nerve activity (Jansen *et al.* 1995; Schreihofer *et al.* 2000).

Excitabilities of RVLM C1 and non-C1 neurons theoretically regulate sympathetic outflows through mono- or polysynaptic connections to sympathetic pre-ganglionic neurons in the spinal cord. Therefore, afferent inputs to the RVLM, which determine the activity levels of C1 and non-C1 neurons, presumably contribute to the regulation of cardiovascular sympathetic outflows. Neuroanatomical (Shafton *et al.* 1998) and electrophysiological (Yang & Coote, 1998) studies revealed that the RVLM receives axonal projections from the paraventricular nucleus of the hypothalamus (PVN). Neurons constituting this monosynaptic pathway (PVN-RVLM neurons) exhibit slow spontaneous discharges that are temporally correlated with renal sympathetic nerve activity in rats (Chen & Toney, 2010). Thus, PVN-RVLM neurons are considered part of the major circuitry that controls the sympathetic vasomotor system. Nonetheless, no study has yet demonstrated that excited PVN-RVLM neurons drive sympathoexcitation. This monosynaptic pathway has attracted considerable research attention as hypothesized to be involved in the chronic sympathetic hyperactivation seen in pathological conditions such as heart failure (Xu *et al.* 2012), as well as in acute sympathetic adjustments to stressors (Dampney 2015). Consequently, the causal relationships that may exist between PVN-RVLM neurons and sympathoexcitation are deserving of further study.

The present study investigated the sympathoexcitatory role of PVN-RVLM neurons in mammals using optogenetic techniques, which allowed us to control excitabilities of a neuronal population of interest (Yizhar *et al.* 2011). We optogenetically stimulated the PVN-RVLM monosynaptic pathway in anaesthetized rats and examined the effects on renal sympathetic nerve activity and other cardiovascular parameters. We also performed neural tract tracing to study the innervation of PVN-RVLM glutamatergic neuronal axons to RVLM C1 neurons.

Methods

Ethical approval

All procedures outlined in this study complied with *Guiding Principles for the Care and Use of Animals in the Fields of Physiological Sciences* published by the Physiological Society of Japan and 'Principles and standards for reporting animal experiments in *The Journal of Physiology* and *Experimental Physiology*' published by the Physiological Society (Grundy, 2015). The procedures were approved by the Animal Care Committee (reference no.: 15-Y-40) and the Gene Recombination Experiment Safety Committee (reference no.: h28-034 and h29-074) of Tottori University. The experiments were performed on 37 male Sprague–Dawley rats. The rats were housed in standard cages in a temperature-controlled room (25°C) with a 12:12 h light–dark schedule. Food and water were made available *ad libitum*.

Viral injection

Our optogenetic approach to gaining control over PVN-RVLM neuron excitability made use of an AAV vector to express the channelrhodopsin variant ChIEF fused with tdTomato under the control of cytomegalovirus promotor (pAAV2-CMV-ChIEF-tdTomato) (Kataoka *et al.* 2014) and an engineered retrograde AAV vector (Tervo *et al.* 2016) to express the humanized channelrhodopsin H134R mutant fused with green fluorescent protein (GFP), under the control of the synapsin promoter (pAAV-Syn-ChR2(H134R)-GFP, a gift from Edward Boyden; 58880-AAVrg, Addgene, Cambridge, MA, USA). The control virus vector constructs, pAAV2-CMV-palGFP (Kataoka *et al.* 2014) and pAAV-hSyn-EGFP (a gift from Bryan Roth; 50465-AAVrg, Addgene), were also used.

The final titrations were 5.35×10^{10} and 1.88×10^{10} GC ml^{-1} for AAV2/1-CMV-ChIEF-tdTomato and AAV2/1-CMV-palGFP, respectively, and 8.0×10^{12} and 7.4×10^{12} GC ml^{-1} for retrograde AAV-Syn-ChR2-GFP and AAV-hSyn-EGFP, respectively.

Rats (>7 weeks old) were anaesthetized with <4% isoflurane in oxygen and were placed in a stereotaxic head unit (900LOS; David Kopf Instruments, Inc., Tujunga, CA, USA, or SR-6R; Narishige, Tokyo, Japan). For unilateral microinjection into the PVN with AAV2/1-CMV-palGFP ($n = 6$, palGFP rats) or AAV2/1-CMV-ChIEF-tdTomato ($n = 22$, ChIEF-tdTomato rats), lidocaine hydrochloride (Xylocaine® jelly 2%, AstraZeneca, Cambridge, UK) was topically applied to the exposed skull and a small burr hole was made in the skull. Then, a glass micropipette filled with the AAV solution was vertically inserted into the brain. The rats received a pressure microinjection of the solution (46.0 nl $\times$ 4 injections) unilaterally into the PVN using a calibrated microinjection system (Nanoject II; Drummond Scientific, Co., Broomall, PA, USA). The coordinates for the injections into the PVN were determined as per the Paxinos and Watson atlas (2007) as 1.9 mm caudal, 0.3 mm lateral and 7.9–8.2 mm ventral to bregma. In 10 of the 22 ChIEF-tdTomato rats that would be employed for Experiment 2, we vertically inserted a 200 μm-thick multimode optical fibre (numerical aperture 0.50, Thorlab, Newton, NJ, USA) for illumination of the PVN. Following insertion into the brain, the fibre was secured using two screws and dental acrylic. The fibre tip was positioned 7.0–7.5 mm ventral to bregma, in the thalamic nucleus reuniens (Re), as confirmed by a scar (Fig. 4*A*).

Other subsets of anaesthetized rats were subjected to bilateral microinjections into the RVLM of retrograde AAV-Syn-ChR2-GFP ($n = 4$, ChR2-GFP$_{retro}$ rats) or AAV-hSyn-EGFP ($n = 5$, EGFP$_{retro}$ rats). The dorsal surface of the medulla was exposed by a midline incision made through the skin covering the back of the head, dissection of the muscles overlaying the base of the skull and an incision made through the atlanto-occipital membrane. The micropipette of the calibrated microinjection system was set at an angle vertical to the dorsal surface of the medulla with the aid of a microscope. Each rat received a pressure microinjection of the AAV vector (23.0 nl $\times$ 6 injections) into the RVLM bilaterally. The coordinates for the RVLM were 1.0 mm rostral and 1.7–1.8 mm lateral to the calamus scriptorius and 3.2–3.5 mm ventral to the dorsal surface of the medulla, in accordance with those reported previously (Koba *et al.* 2014). The rats post-operatively received administration of an antibiotic (cefazolin, 15 mg kg^{-1}, I.M., Astellas Pharma, Tokyo, Japan) and the skin wounds were disinfected by topical application of iodine (Mundipharm, Limburg an der Lahn, Germany) and an ointment containing chlorhexidine (Oronine H ointment, Otsuka

Pharmaceutical, Tokyo, Japan). After the surgery, the rats were housed in a standard cage for a minimum of 2 weeks prior to the experiment day. The rats received a daily health check and we were prepared to treat the animals with analgesics in the case that any of them displayed any signs of inflammation, discomfort, anxiety or pain; however, none of them needed to be treated with analgesics or additional interventions.

Surgery and optogenetic experiments

In Experiment 1, we photostimulated the RVLM in ChIEF-tdTomato rats. This involved optogenetic stimulation of axonal fibres of PVN-RVLM neurons and examination of the effects on sympathetic vasomotor tone. palGFP ($n = 6$) and ChIEF-tdTomato ($n = 12$) rats were anaesthetized with a mixture of <4% isoflurane and oxygen. The trachea was cannulated and the lungs were artificially ventilated using a respirator (SN480-7, Shinano, Tokyo, Japan) with a 6 ml kg^{-1} tidal volume at a frequency of 60–70 breaths per min. The right femoral artery and vein were cannulated to measure arterial pressure (AP) and to administer drugs, respectively. The arterial catheter was attached to a pressure transducer (P23XL; Becton Dickinson and Co., Franklin Lakes, NJ, USA). Two needle electrodes were placed on the forelimbs to record analog electrocardiogram (ECG) signals, which were amplified using an amplifier (MEG-5200, Nihon Kohden Corp., Tokyo, Japan). Heart rate (HR) as well as mean AP (MAP) were calculated beat-to-beat with detection of the interval time between successive R waves in the ECG. Then, the rats were placed in the stereotaxic apparatus. Body core temperature, measured rectally, was maintained at 36.0∼37.5°C with a heating pad and lamp. To measure renal sympathetic nerve activity (RSNA), a bipolar electrode made of a Teflon-insulated stainless steel wire (790600; A-M Systems, Inc., Sequim, MA, USA) was attached to the renal nerve directed to the left kidney and fixed with a silicone adhesive (Kwik-Sil, World Precision Instruments, Sarasota, FL, USA). The RSNA signal was amplified through the amplifier with a bandpass low-frequency of 150 Hz and a high-frequency filter of 1 kHz and made audible. For photostimulation of the RVLM ipsilateral to the PVN that received the AAV injection, the dorsal surface of the brainstem was exposed. Then, a 200 μm-thick multimode optical fibre (Thorlab), connected to a 473 nm wavelength diode-pumped solid-state laser (BL473T8-200, Shanghai Laser and Optics Co., Shanghai, China) controlled by a pulse generator (STOmk-2, BRC Co., Nagoya, Japan), was inserted into the brainstem at an angle vertical to the dorsal surface of the brainstem with the aid of the microscope. Prior to the insertion, laser output measured at the tip of the fibre with a light power metre (LPM-100, BRC Co.) was set at 9∼10 mW when the laser was activated in a

continuous mode. The stereotaxic coordinates for the tip of the fibre were 1.0 mm rostral and 1.8–2.0 mm lateral to the calamus scriptorius and 2.7 mm ventral to the dorsal surface of the medulla. Thus, the fibre tip was positioned at 0.5–1.0 mm dorsocaudal from the target RVLM. This was confirmed *post hoc* by the location of a scar made by repeatedly inserting and removing the optic fibre into the brain (Fig. 2*A*).

Upon completion of the surgery, the rats were intravenously given an initial dose of urethane (600 mg kg^{-1}) and α-chloralose (60 mg kg^{-1}) under artificial ventilation with 1% isoflurane in oxygen. Ten to fifteen minutes later, the rats were removed from isoflurane and the ventilator and allowed to breathe spontaneously with room air. Supplemental doses of the mixture of urethane and α-chloralose were intravenously given to maintain anaesthesia as necessary. Adequacy of anaesthesia was confirmed by the absence of a withdrawal reflex response to nociceptive stimulation of a hind paw throughout the surgery and experimental protocols. At least 60 min was allowed after withdrawal of isoflurane. Then, 2 min photostimulation with light pulses at 10 Hz with 50 ms pulse duration, 20 Hz with 10 ms pulse duration, or 40 Hz with 5 ms pulse duration was given to the RVLM with simultaneous recordings of RSNA, AP and HR. The order of stimulation frequency was random and intervals of at least 20 min were allowed between the manoeuvres.

In Experiment 2, we examined the effect of glutamate receptor blockade in the RVLM on PVN stimulation-elicited sympathoexcitation. In 6 of 10 ChIEF-tdTomato rats in which optical fibres had been implanted for photostimulation of the PVN, AAV was successfully microinjected as confirmed *post hoc* by a substantial number of tdTomato-labelled neurons localized in the PVN (Fig. 4*A*). The rats were subjected to the surgery to measure AP, ECG and RSNA, as conducted in Experiment 1. After more than 60 min after withdrawal of isoflurane, saline (46.0 nl) or a cocktail solution of 2-amino-5-phosphonopentanoic acid (AP5; A5282, Sigma-Aldrich, St Louis, MO, USA) and water-soluble 6-cyano-7-nitro-quinoxaline-2,3-dione (CNQX; ab120044, Abcam, Cambridge, UK) (10 mM for each, 46.0 nl in saline) was unilaterally microinjected into the RVLM ipsilateral to the PVN with the fibre implantation. The dosages contained within the cocktail were determined based on previous studies (Wang *et al.* 2009; Kataoka *et al.* 2014). Ten to fifteen minutes later, unilateral photostimulation of the PVN was given for 2 min at 40 Hz with a 5 ms pulse duration. In 4 of 6 rats, PVN stimulation-elicited changes in RSNA, MAP and HR were again examined 60–70 min after the AP5/CNQX microinjection. After data collection, the pipette for microinjection into the RVLM was repetitively inserted into and removed from the brain to make scars for *post hoc* confirmation of the location of the pipette tip (Fig. 4*B*).

In Experiment 3, we investigated changes in RSNA, MAP and HR in response to photostimulation of the PVN of ChR2-GFP$_{retro}$ rats, i.e. optogenetic stimulation of cell bodies/dendrites of PVN-RVLM neurons. In EGFP$_{retro}$ ($n = 5$) and ChR2-GFP$_{retro}$ ($n = 4$) rats, surgery to measure AP, ECG and RSNA was conducted as described above. An optical fibre for bilateral photostimulation of the PVN was inserted into the brain 1.9 mm caudal, 0.0–0.2 mm lateral to the midline (so as not to damage superior cerebral veins in the superior sagittal sinus) and 7.0–7.5 mm ventral to the bregma (Fig. 5*B*). Ten to fifteen minutes after intravenous infusion of the mixture of urethane and α-chloralose, the rats were removed from the isoflurane but were still maintained under artificial ventilation. After more than 60 min following withdrawal of isoflurane, changes in RSNA, AP and HR in response to 1 min intermittent bouts (0.5 s pulse illumination with a 1.5 s interval, 30 bouts) of photostimulation of the PVN at 10, 20 or 40 Hz with a 5 ms pulse duration were examined under artificial ventilation. Lung inflation-induced vagal afferent activity mediates respiratory cycle-synchronized sympathetic nerve discharges (Häbler *et al.* 1994). Thus, the effect of lung inflation-entrained sympathetic outflow on RSNA changes in response to the periodic photostimulation (every 2 s) needed to be randomized. To achieve this, the frequency for the artificial ventilation during data collection was set at 70 breaths min^{-1}, which was not synchronized with that for the periodic photostimulation. After data collection, as performed in Experiment 1 and 2, a scar was made to label the location of the fibre tip (Fig. 5*B*).

At the conclusion of the above experiments, the renal nerve was cut between the electrode and the neural axis to measure the background noise of RSNA. Then, the rats were deeply anaesthetized with an additional intravenous infusion of urethane and α-chloralose and transcardially perfused with saline followed by 4% paraformaldehyde in 0.1 M phosphate-buffered saline (PBS; pH 7.4). For histology, the brains were removed and postfixed for 4–12 h in 4% paraformaldehyde and then cryoprotected in a 30% sucrose solution at 4°C for 24–48 h. Then, 30 μm-thick coronal sections were prepared with a cryostat (CM1900, Leica, Wetzlar, Germany) for immunofluorescence staining as below.

Immunofluorescence staining

Immunofluorescence staining was performed in accordance with previously described methods (Kumada *et al.* 2017). Briefly, the tissue sections were washed in PBS (2 × 10 min) and incubated in an incubation solution (PBS containing 0.3% Triton X-100, 2.5 g l^{-1} lambda carrageenan, 200 mg l^{-1} NaN$_3$, 10 ml l^{-1} normal donkey or goat serum) for 2 h at room temperature. Then, the sections were incubated in the solution with primary

antibodies for 18–42 h on a shaker at 4°C. The primary antibodies used in this study were goat anti-tdTomato antibody (1:500, AB8181, Sicgen, Cantanhede, Portugal), goat (1:1000, GTX26673, GeneTex, Irvine, CA, USA) or rabbit (1:4000, GTX113617, GeneTex) anti-GFP antibody, rabbit anti-vesicular glutamate transporter 1 (VGLUT1) antibody (1:250, AF500, Frontier Institute Co., Ltd, Ishikari, Japan), rabbit anti-VGLUT2 antibody (1:500, AF860, Frontier Institute Co., Ltd) and rabbit (1:1000, AB152, Merck Millipore, Billerica, MA, USA) or chicken (1:1000, ab76442, Abcam) anti-tyrosine hydroxylase (TH) antibody. The sections were rinsed in PBS containing 0.03% Triton X-100 (2 × 10 min) and incubated in the incubation solution with secondary antibodies. The secondary antibodies used were Alexa Fluor 488-conjugated donkey anti-chicken antibody (1:500, 703-545-155, Jackson ImmunoResearch, West Grove, PA, USA), Alexa Fluor 555-conjugated goat anti-chicken antibody (1:500, ab150174, Abcam), Alexa Fluor 555-conjugated donkey anti-goat antibody (1:500, A-21432, Thermo Fisher Scientific, Waltham, MA, USA), Alexa Fluor 405- (1:500, ab175649, Abcam) or Alexa Fluor 488-conjugated (1:500, A-21206, Thermo Fisher Scientific) donkey anti-rabbit antibody and Alexa Fluor 488-conjugated goat anti-rabbit antibody (1:500, ab150077, Abcam). Then, the sections were mounted on slides and coverslipped using Prolong Gold antifade reagent (P36930, Thermo Fisher Scientific). The sections were observed and digital images were captured using a digital fluorescence microscope (BZ-9000, Keyence, Osaka, Japan) or confocal fluorescence microscopy (LSM780, Carl Zeiss, Oberkochen, Germany).

Data acquisition and statistical analyses

Throughout surgery and data collection for photo-stimulation experiments, all measured variables were displayed on a computer monitor and stored on a hard disk via analog-to-digital conversion (Powerlab/8s; ADInstruments, Dunedin, New Zealand) at a sampling rate of 1 kHz. MAP and HR, obtained beat-by-beat, were resampled at 1 kHz and averaged over 1 s.

To quantify the RSNA responses to photostimulation, full-wave-rectified signals of RSNA, as well as background noise signals, were obtained; then the noise component for RSNA was subtracted from the rectified signal. The RSNA responses to 2 min photostimulation in Experiments 1 and 2 were quantified every 1 s as relative changes in RSNA from baseline levels. Basal values obtained from mean values during the 60 s immediately prior to photo-stimulation were denoted as 100%. To quantify RSNA in response to a short period (0.5 s) of photostimulation during the 1 min intermittent stimulation protocol in Experiment 3, additional procedures were conducted

using a modification of a previously described method (Koba et al. 2009). Relative changes in RSNA from the base-line, sampled at 1 kHz in response to each period of 0.5 s photostimulation, were averaged over 10 ms; then, those values were superimposed on one another and averaged (Fig. 5E). Values of area under the curve (AUC) of the averaged RSNA changes were also calculated as an index of RSNA response to photostimulation by integrating the increases in averaged RSNA from baseline during the time period (Fig. 5E).

Data are expressed as means ± SEM. To assess the significant differences, data were analysed with Student's paired (within the same animals) and unpaired (between rat groups) t test (Microsoft Excel 2013) and one-way ($vs.$ basal values) or two-way (photostimulation frequency × rat group) repeated measures ANOVA followed by Dunnet's or Tukey's $post$ hoc test (SigmaPlot for Windows 11.2.0.5, Systat Software Inc., San Jose, CA, USA). $P < 0.05$ was considered statistically significant.

Results

Experiment 1: effects of photostimulation of axonal fibres of PVN-RVLM neurons on renal sympathetic nerve activity

Four of six palGFP and 14 of 22 ChIEF-tdTomato rats successfully received unilateral microinjection of AAV vectors within the PVN, as confirmed with palGFP or tdTomato expression in PVN neurons (Fig. 1A). In these rats, $post$ hoc immunofluorescence staining revealed that the palGFP- or tdTomato-labelled axons derived from the PVN were distributed in the RVLM, in which tyrosine hydroxylase-immunoreactive C1 cells were also distributed (Fig. 1B). Moreover, the PVN-derived axons were more abundant in the RVLM ipsilateral to the side of AAV injection in the PVN than the contralateral side (Fig. 1B), consistent with a previous study (Stocker et al. 2006).

In anaesthetized palGFP ($n = 4$) and ChIEF-tdTomato ($n = 8$) rats that had AAV microinjection into the PVN, basal values of signal-to-noise ratio (SNR) for RSNA, MAP and HR before 2 min photostimulation of the ipsilateral RVLM did not significantly differ between the rat groups and among the protocols (Table 1). The palGFP rats exhibited no changes in RSNA, MAP and HR in response to 2 min photostimulation of the RVLM at 10, 20 or 40 Hz (Fig. 2B and D). In contrast, the ChIEF-tdTomato rats exhibited significant increases in RSNA and MAP from the baseline in response to photostimulation of the RVLM at 20 or 40 Hz. These responses lasted even after stimulation offset (Fig. 2C and E). Photostimulation of the RVLM of the ChIEF-tdTomato rats at 10 Hz elicited modest and slow increases in RSNA and MAP (Fig. 2E). HR did not significantly change from the baseline during

Table 1. Basal values of sympathetic cardiovascular parameters in anaesthetized palGFP and ChIEF-tdTomato rats immediately before 2 min photostimulation of the RVLM and animal characteristics on the experimental day for Experiment 1

	palGFP			ChIEF-tdTomato		
	10 Hz	20 Hz	40 Hz	10 Hz	20 Hz	40 Hz
Signal-to-noise ratio for RSNA	1.54 ± 0.19	1.56 ± 0.18	1.60 ± 0.18	1.62 ± 0.11	1.56 ± 0.10	1.55 ± 0.10
MAP (mmHg)	114 ± 3	110 ± 4	111 ± 2	110 ± 3	111 ± 2	112 ± 3
HR (bpm)	358 ± 30	364 ± 32	367 ± 32	356 ± 20	355 ± 16	362 ± 12
No. of animals		4			8	
Age (weeks)		11.0 ± 0.4			11.0 ± 0.4	
Body weight (g)		361 ± 7			399 ± 17	
Weeks after AAVs injection		3.1 ± 0.4			3.4 ± 0.4	

photostimulation. Nevertheless, slight but significant tachycardic responses were observed after the offset of photostimulation at 10 and 40 Hz. The RSNA responses in ChIEF-tdTomato rats, as assessed by integration of the changes from the baseline during photostimulation, were dependent on the frequency of the light pulses given (Fig. 2F).
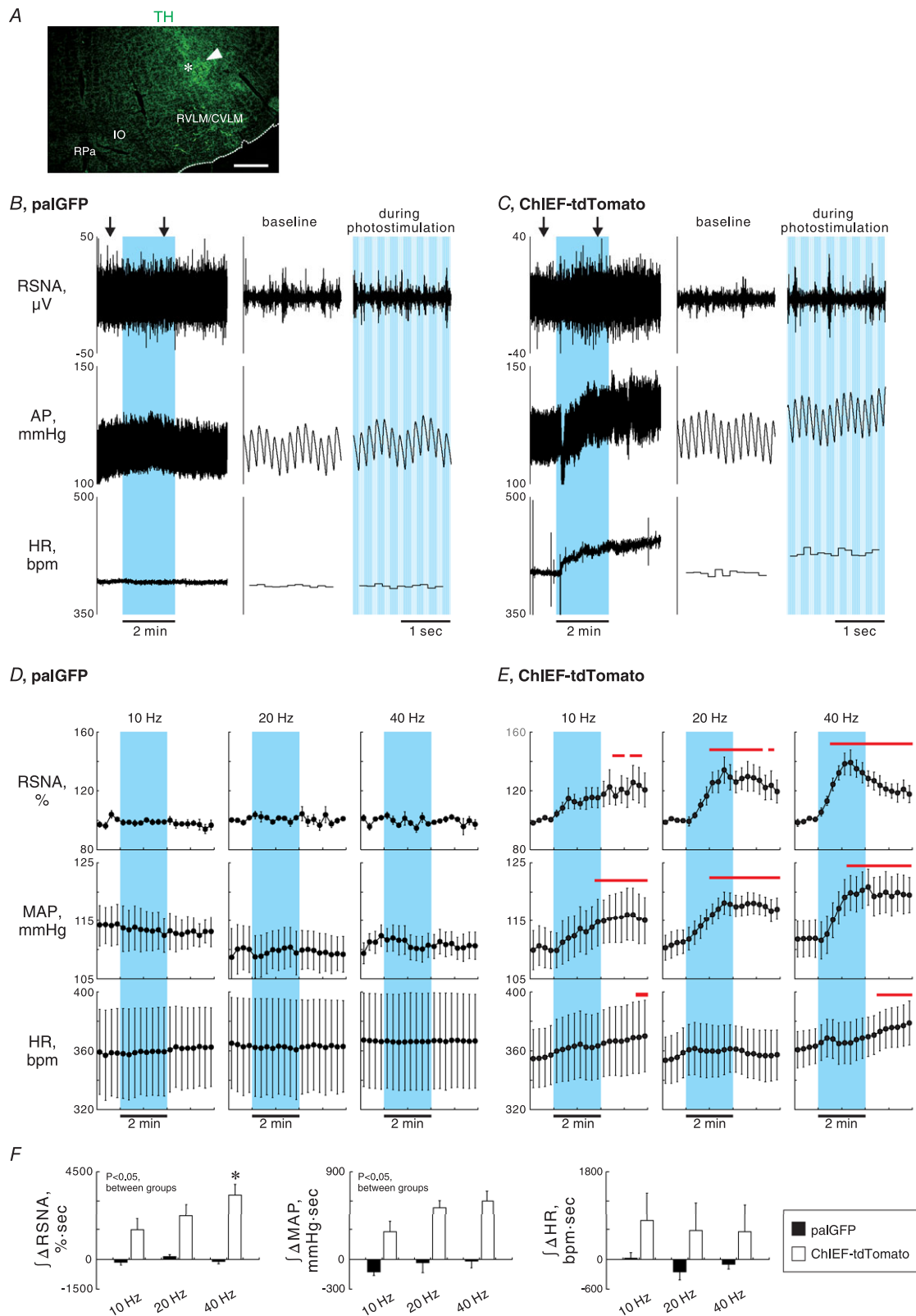
In two palGFP and four ChIEF-tdTomato rats where AAV injections missed the PVN, no GFP- or tdTomato-labelled axons were observed in the RVLM, and photostimulation of the RVLM never elicited the sympathetic cardiovascular responses.

Double immunofluorescence staining/confocal microscopy in the RVLM of ChIEF-tdTomato rats with AAV injection right into the PVN revealed tdTomato-labelled, PVN-derived axons that contained VGLUT2, but not VGLUT1 (Fig. 3A), consistent with a previous study (Stocker *et al.* 2006). Moreover, triple immunofluorescence staining visualized swellings of VGLUT2-containing, PVN-derived axons (i.e. boutons terminaux), which were closely associated with cell bodies and dendrites of tyrosine hydroxylase-immunoreactive RVLM C1 neurons (Fig. 3B). These confocal observations suggest that PVN-RVLM glutamatergic
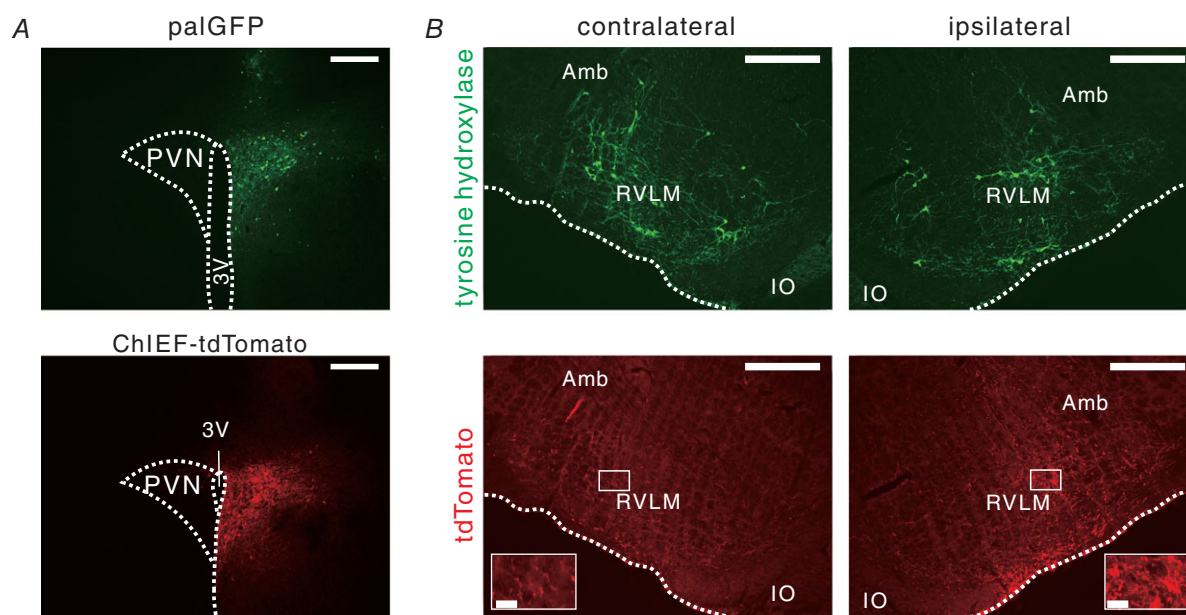
Figure 1. Fluorescence images of brain sections of palGFP and ChIEF-tdTomato rats
A, hypothalamic coronal sections of palGFP (upper) and ChIEF-tdTomato (lower) rats, showing AAV transductions of PVN neurons (autofluorescence). Scale bars: 500 μm. 3V, third ventricle. *B*, a medullary coronal section obtained from the ChIEF-tdTomato rat, showing distribution of tyrosine hydroxylase (TH, upper) and tdTomato (lower) immunoreactivities in the ventrolateral medulla contralateral (left) and ipsilateral (right) to the PVN into which the AAV vector had been unilaterally microinjected. Insets in the lower panels magnify the areas indicated by the squares in the RVLM. The rostrocaudal level of this section was immediately caudal to the caudal pole of the facial nucleus. Scale bars: 500 μm and 50 μm (insets). Amb, nucleus ambiguus; IO, inferior olivary complex.

Figure 2. Sympathoexcitation by photostimulation of the nerve terminals of PVN-RVLM neurons

A, a medullary coronal section showing TH immunoreactivity and the scar (arrowhead) and wreck (asterisk) made due to an insertion of an optical fibre. Scale bar: 500 μm. The rostrocaudal level of this section was approximately 1 mm caudal to the caudal pole of the facial nucleus. CVLM, caudal ventrolateral medulla; RPa, raphe pallidus

neurons containing VGLUT2 form synaptic contacts with RVLM C1 neuronal cells, leading to the hypothesis that the sympathoexcitation that was elicited by photostimulation of PVN-RVLM neurons was mediated by the mono-synaptic glutamatergic transmission to the RVLM.

Experiment 2: effects of glutamate receptor blockade in the RVLM on PVN photostimulation-elicited renal sympathoexcitation

To test the hypothesis stated above, we examined the effects of blockade of glutamatergic synapses in the RVLM on sympathetic cardiovascular responses elicited by photo-stimulation of PVN cell bodies. Saline or a cocktail of AP5 and CNQX, glutamate receptor blockers, was unilaterally microinjected into the RVLM ipsilateral to AAV injection into the PVN in anaesthetized ChIEF-tdTomato rats, and subsequently, 2 min photostimulation was given to the PVN (Fig. 4A and B). In ChIEF-tdTomato rats that received successful AAV microinjection ($n = 6$, 10.9 $\pm$ 0.4 weeks of age, 372 $\pm$ 17 g of body weight, 2.1 $\pm$ 0.1 weeks after AAV microinjection), basal values of SNR for RSNA, MAP and HR 10–15 min after saline injection into the RVLM (2.21 $\pm$ 0.22, 108 $\pm$ 4 mmHg and 391 $\pm$ 4 beats per minute (bpm)) did not significantly differ from those obtained after AP5/CNQX injection into the RVLM (2.33 $\pm$ 0.16, 108 $\pm$ 5 mmHg and 372 $\pm$ 14 bpm; $P > 0.05$). After saline injection, photostimulation of the PVN significantly elevated RSNA from baseline, but did not change MAP or HR (Fig. 4C). Ten to fifteen minutes after AP5/CNQX injection into the RVLM, PVN photo-stimulation exerted no significant effects on RSNA, MAP or HR (Fig. 4C). The RSNA changes during the PVN photostimulation, as assessed by integration of changes from baseline during photostimulation, were significantly smaller after AP5/CNQX injection into the RVLM than those observed after saline injection (Fig. 4D). No pressor or tachycardic response to photostimulation of the PVN may be explained by excitations of PVN-RVLM neurons and other sympathoexcitatory PVN neurons but also sympathoinhibitory neurons in the PVN. In 4 of 6 rats, RSNA, AP and HR changes in response to photostimulation of the PVN were examined 60–70 min after AP5/CNQX injection into the RVLM (basal values: 2.53 $\pm$ 0.14, 113 $\pm$ 11 mmHg, 384 $\pm$ 3 bpm). The renal

sympathoexcitatory response to PVN photostimulation was partially restored in these rats. The integrated changes in RSNA from baseline during photostimulation tended to increase from those at 10–15 min after AP5/CNQX injection ($+514 \pm 249\%$ s, $P < 0.07$).

Experiment 3: effects of intermittent photostimulation of PVN-RVLM neuronal cell bodies on renal sympathetic nerve activity

All of five EGFP$_{retro}$ and four ChR2-GFP$_{retro}$ rats were confirmed as receiving bilateral microinjections of retrograde AAV vectors in the RVLM (Fig. 5A). In these rats, GFP-labelled neuronal cell bodies and dendrites were found in the PVN via *post hoc* immunofluorescence staining (Fig. 5B). Basal values of SNR for RSNA, MAP and HR before photostimulation did not significantly differ between the rat groups and among the protocols (Table 2). In ChR2-GFP$_{retro}$ rats, 1 min intermittent bouts (0.5 s illumination pulses with a 1.5 s interval; Fig. 5C and D) of photostimulation elicited renal sympathoexcitation synchronous with each bout of 0.5 s illumination pulses (Figs. 5C–E and 6B). Superimposing analyses conducted over 30 bouts of stimulation (Fig. 5E) revealed that photostimulation at 10, 20 or 40 Hz elicited significant renal sympathoexcitation, followed by a rapid return to basal levels or sympathoinhibition in ChR2-GFP$_{retro}$, but not in EGFP$_{retro}$, rats (Fig. 6A and B). It was noted that when photostimulation at 10 Hz, but not at 20 or 40 Hz, was given to the PVN of ChR2-GFP$_{retro}$ rats, RSNA responded to each photo-pulse as shown by five peaks in RSNA during a stimulation cycle consisting of five photo-pulses (Figs. 5E and 6B). The intensity of the renal sympathoexcitatory responses to photostimulation in ChR2-GFP$_{retro}$ rats, assessed by AUC (Fig. 5E), was independent of the stimulation frequency (Fig. 6C). Five second-averaged time courses of MAP and HR indicated no significant changes from baseline in MAP or HR during the 1 min intermittent stimulation periods in EGFP$_{retro}$ and ChR2-GFP$_{retro}$ rats (Fig. 6D and E). It is possible that no changes in MAP and HR occurred because each period of sympathoexcitation, intermittently elicited by 0.5 s illumination pulses, was too short to change the level of MAP or HR.

nucleus. B and C, representative traces of renal sympathetic nerve activity (RSNA), arterial pressure (AP) and heart rate (HR) while 2 min photostimulation at 40 Hz with 5 ms pulse duration was unilaterally given to the RVLM ipsilateral to the side of AAV injection into the PVN (blue background), obtained from palGFP (B) and ChIEF-tdTomato (C) rats. Traces at baseline and during photostimulation (arrows in the left panels) are magnified in the right panels. bpm, beats per minutes. D and E, 15 s-averaged time courses of RSNA, mean AP (MAP) and HR in 4 palGFP (D) and 8 ChIEF-tdTomato (E) rats while photostimulation was given to the RVLM for 2 min at 10 Hz with 50 ms pulse duration (PD), 20 Hz with 10 ms PD or 40 Hz with 5 ms PD. Values are means $\pm$ SEM. Horizontal red bars, $P < 0.05$ *vs.* baseline. F, comparisons between the rat groups and among the photostimulation frequencies of RSNA, MAP and HR responses to photostimulation of the RVLM, assessed by integration of changes from baseline during 2 min photostimulation. *$P < 0.05$ *vs.* 10 Hz.

Discussion

The present study provides the first direct evidence that excited PVN-RVLM neurons drive sympathoexcitation. We found that photostimulation of either RVLM nerve endings derived from ChIEF-tdTomato-expressing neurons in the PVN or PVN cell bodies transduced with ChR2-GFP by retrograde infection of AAV injected into the RVLM elicited renal sympathoexcitatory responses. Moreover, our immunofluorescence confocal microscopy revealed that PVN-RVLM neuronal axons containing VGLUT2 immunoreactivity were closely associated with tyrosine hydroxylase-positive cells in the RVLM, suggesting that PVN-RVLM glutamatergic neurons form synaptic contacts with RVLM C1 neurons. Glutamatergic transmission in the RVLM is involved in regulation of the sympathetic nervous system (Guyenet, 2006). RVLM C1 neurons are endowed with ionotropic glutamate receptor subunits (Brailoiu *et al.* 2002) and have been shown to play a sympathoexcitatory role (Morrison *et al.* 1988; Jansen *et al.* 1995; Abbott *et al.* 2009). These previous and present findings all support the possibility that the monosynaptic glutamatergic transmission from PVN neurons to RVLM C1 neurons is part of the central processes that increase cardiovascular sympathetic outflows. This view is further supported by our present experiments in which renal sympathoexcitation elicited by photostimulation of PVN cell bodies was suppressed by blockade of ionotropic glutamate receptors in the RVLM. Taken together, we propose that the monosynaptic glutamatergic transmission through the PVN-RVLM pathway helps drive cardiovascular sympathoexcitation via stimulation of RVLM C1 neurons.

RVLM non-C1 neurons are also known to express ionotropic glutamate receptors (Brailoiu *et al.* 2002) and help generate sympathetic nerve activity (Jansen *et al.* 1995; Schreihofer *et al.* 2000). It is conceivable that RVLM non-C1 neurons, potentially VGLUT2-expressing, spinal projecting excitatory neurons (Stornetta *et al.* 2002), are also a direct downstream target of the PVN-RVLM glutamatergic neurons although there exists no empirical evidence to support this hypothesis. Therefore, stimulation of RVLM non-C1 neurons might also contribute to the sympathoexcitation driven by excitation of PVN-RVLM glutamatergic neurons. However, it remains unclear whether RVLM non-C1 neurons play a more or less sympathoexcitatory role than RVLM C1 neurons when this monosynaptic pathway is engaged.

Optogenetic stimulation of PVN-RVLM neurons

In the present study, we used two optogenetic approaches to stimulate PVN-RVLM neurons. The first was projection axonal targeting (Yizhar *et al.* 2011), involving transduction of PVN cells with ChIEF-tdTomato. This resulted in labelling of many PVN-derived axonal terminals in the RVLM with tdTomato (Fig. 1*B*). Thus, photostimulation given to the RVLM of ChIEF-tdTomato rats likely stimulated axonal fibres of PVN-RVLM neurons. In the second approach, we employed a recently developed optogenetic technique using retrograde AAV infection at axon terminals (Tervo *et al.* 2016). In the present study, retrograde AAV vectors injected in the RVLM were transported back through PVN-RVLM axons, as evidenced by
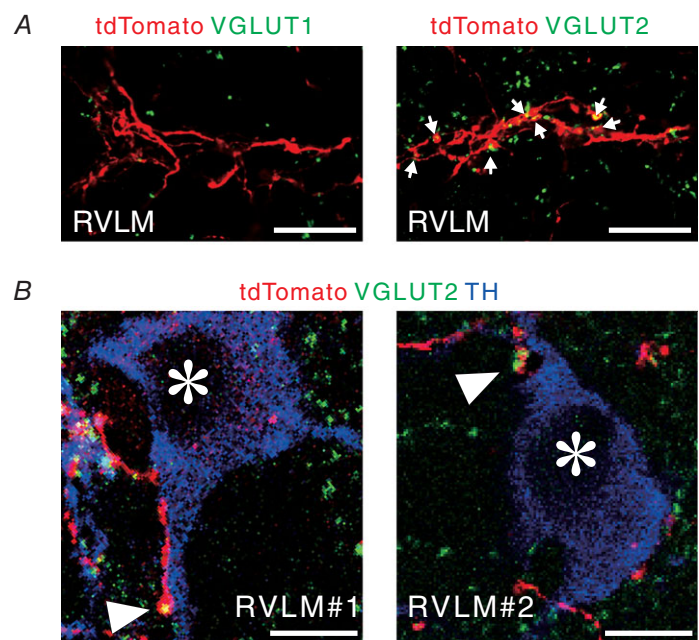
Figure 3. Close association of PVN-RVLM glutamatergic neurons with RVLM C1 neurons
*A*, pseudocoloured confocal images showing that PVN-derived, tdTomato-immunoreactive axons contained VGLUT2 immunoreactivity (right, arrows), but not VGLUT1 immunoreactivity (left) in the RVLM of a ChIEF-tdTomato rat. Scale bars: 20 μm. *B*, pseudocoloured confocal images showing that PVN-derived, tdTomato-immunoreactive axonal swellings (arrowheads) containing VGLUT2 immunoreactivity were apposed to TH-immunoreactive cell bodies (asterisk) in the RVLM of ChIEF-tdTomato rats. Two examples are shown. Scale bars: 10 μm.

GFP immunoreactivities in the cell bodies and dendrites of PVN neurons (Fig. 5*B*). Thus, photostimulation of the PVN of ChR2-GFP$_{retro}$ rats was considered to optogenetically stimulate the cell bodies/dendrites of PVN-RVLM neurons transduced with ChR2-GFP.

The RVLM not only receives axonal projections from the PVN, but also innervates the PVN (RVLM-PVN neurons) (Cunningham *et al.* 1990). In Experiment 1, since the AAV2/1 vectors reportedly afford some degree of low-efficiency, retrograde access to projection neurons in selected neural circuits (Zingg *et al.* 2017), ChIEF-tdTomato might also be expressed in RVLM-PVN neurons of ChIEF-tdTomato rats. However, we observed no immunoreactivities for the reporter proteins tdTomato or palGFP in cell bodies in the ventral medulla of ChIEF-tdTomato or palGFP rats (Figs. 1*B* and 3*A*). Thus, the sympathoexcitation elicited by photostimulation of the RVLM in ChIEF-tdTomato rats was unlikely to be caused by stimulation of RVLM-PVN neurons.

Besides PVN-RVLM neurons, the PVN contains cells that monosynaptically target the spinal intermediolateral cell column (IML; PVN-IML neurons), where cell bodies of sympathetic preganglionic neurons are located, and cells that have branched axons and innervate both the RVLM and IML (PVN-RVLM&IML neurons) (Saper *et al.* 1976; Shafton *et al.* 1998; Pyner & Coote, 2000). In Experiment 1, it is possible that photostimulation of the RVLM might stimulate passing PVN-IML neuronal axons since this cell group should send axons to the IML through the medulla. However, axonal fibres of PVN-IML neurons descend along the ventrolateral surface of the medulla (Saper *et al.* 1976; Luiten *et al.* 1985). As the tip of the optical fibre was located dorsocaudally to the RVLM (Fig. 2*A*), the impact of photostimulation on PVN-IML neurons, if any, appears minimal. Moreover, as AAVs used in the present study could transduce PVN-RVLM&IML neurons, we cannot rule out the possibility that PVN-RVLM&IML neurons were stimulated by illumination of the RVLM in ChIEF-tdTomato rats or the PVN in ChR2-GFP$_{retro}$ rats. However, the population of PVN-RVLM&IML neurons is reportedly 5–25% of PVN-RVLM neurons in rats (Pyner
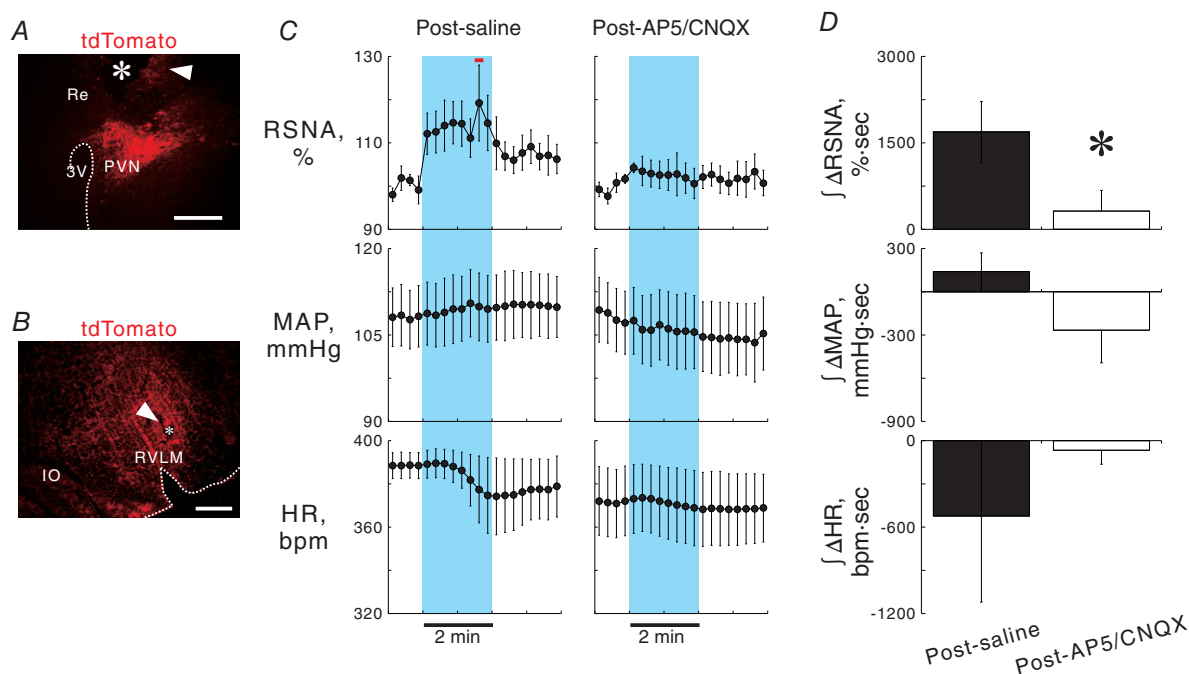

Figure 4. Effect of blockade of ionotropic glutamate receptors in the RVLM on PVN photostimulation-elicited sympathoexcitation
A, a hypothalamic coronal section showing a scar (arrowhead) and a wreck (asterisk) due to chronic implantation of an optical fibre directed to the PVN and tdTomato-positive signals (autofluorescence) in a ChIEF-tdTomato rat. Re, nucleus reuniens in the thalamus. Scale bar: 500 μm. *B*, a medullary coronal section of a ChIEF-tdTomato rat, showing a scar (arrowhead) due to repetitive insertions of the pipette for microinjection in the RVLM, in which PVN-derived, tdTomato-immunoreactive axonal signals were concentrated. Scale bar: 500 μm. *C*, 15 s-averaged time courses of RSNA, MAP and HR in six ChIEF-tdTomato rats while 2 min photostimulation at 40 Hz with 5 ms pulse duration was given to the PVN 10–15 min after saline or a cocktail of AP5 and CNQX was injected into the RVLM. Horizontal red bar, $P < 0.05$ *vs.* baseline. *D*, comparisons of RSNA, MAP and HR changes in response to photostimulation of the PVN after injection into the RVLM with saline or a cocktail of AP5 and CNQX. *$P < 0.05$ *vs.* post-saline.

& Coote, 2000). In addition, Experiment 2 showed that renal sympathoexcitatory responses to photostimulation of PVN cell bodies transduced with ChIEF-tdTomato were suppressed by administration of glutamate receptor blockers into the RVLM. This observation supports the dominant role of PVN-RVLM neurons in driving sympathoexcitation. Overall, although the PVN sends axonal projections not only to the RVLM but also to the spinal IML, the available lines of evidence support the view that PVN-RVLM neurons principally mediate the descending pathway from the PVN that drives renal sympathoexcitation.

In ChIEF-tdTomato rats, renal sympathoexcitation elicited by photositmulation of the PVN (Experiment 2)
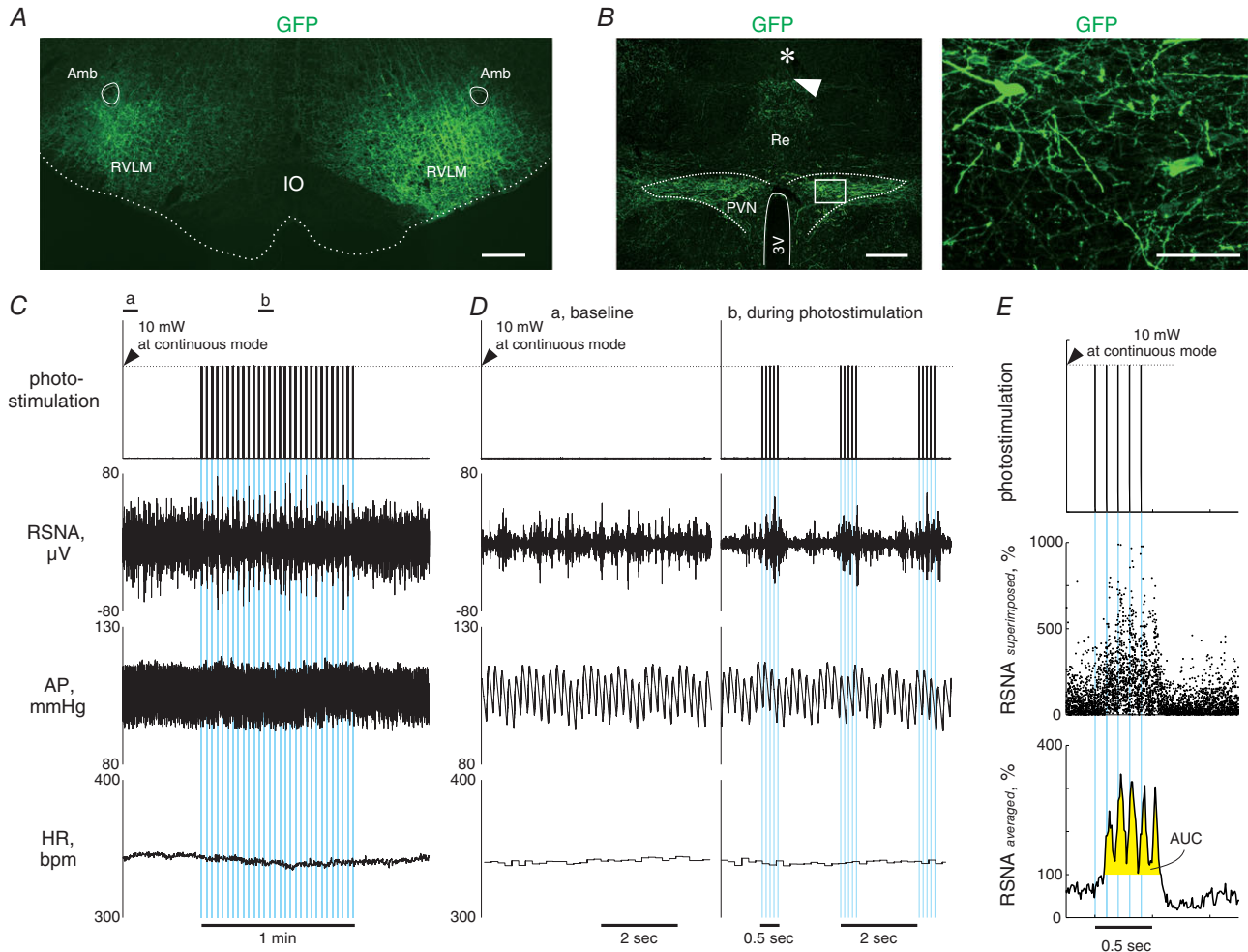
Figure 5. Representatives of fluorescence images of brain sections and photostimulation-elicited sympathetic and cardiovascular responses in ChR2-GFP$_{retro}$ rats

A, a medullary coronal section of a ChR2-GFP$_{retro}$ rat, showing AAV transductions of axonal fibres in the RVLM. Scale bar: 500 μm. *B*, hypothalamic coronal sections of a ChR2-GFP$_{retro}$ rat showing GFP immunoreactivities as well as a scar (arrowhead) and a wreck (asterisk) due to insertions of an optical fibre (left) and microphotographs of GFP immunoreactivities in the PVN (right). The rectangular area in the left panel is magnified in the right panel. Scale bars: 500 μm (left) and 100 μm (right). *C*, representative traces of RSNA, AP and HR as well as the analog DC input to generate blue light output while 1 min intermittent bouts (0.5 s illumination pulses with a 1.5 s interval) of photostimulation at 10 Hz with 5 ms pulse duration was unilaterally given to the PVN (blue background), obtained from a ChR2-GPF$_{retro}$ rat. Each blue background represents one bout of photostimulation given to the PVN, the width of which indicates 500 ms. *D*, traces at baseline and during photostimulation indicated by horizontal bars in *C* are magnified. Each blue background represents one photo-pulse, the width of which is 5 ms. *E*, superimposing analysis performed on the data shown in *C* and *D*. The analog DC input for light output (top) and plots of 10 ms-averaged RSNA (middle) during each cycle for 30 interventions of photostimulation, as well as the averaged RSNA on the 30 plots at each time point during a stimulation-to-non-stimulation cycle (bottom). The values of area under the curve (AUC) for RSNA, an index of the response to photostimulation, were determined as the area coloured yellow.

Table 2. Basal values of sympathetic cardiovascular parameters in anaesthetized EGFP$_{retro}$ and ChR2-GFP$_{retro}$ rats immediately before 1 min intermittent bouts of photostimulation of the PVN and animal characteristics on the experimental day for Experiment 3

	EGFP$_{retro}$			ChR2-GFP$_{retro}$		
	10 Hz	20 Hz	40 Hz	10 Hz	20 Hz	40 Hz
Signal-to-noise ratio for RSNA	2.56 ± 0.27	2.46 ± 0.27	2.36 ± 0.23	2.85 ± 0.42	2.87 ± 0.40	2.84 ± 0.38
MAP (mmHg)	107 ± 5	103 ± 5	103 ± 5	108 ± 5	107 ± 5	110 ± 3
HR (bpm)	382 ± 11	385 ± 14	392 ± 9	353 ± 7	354 ± 9	363 ± 8
No. of animals		5			4	
Age (weeks)		12.3 ± 1.0			13.6 ± 0.3	
Body weight (g)		398 ± 40			434 ± 22	
Weeks after AAVs injection		3.1 ± 0.1			5.4 ± 0.6*	

*$P < 0.05$ *vs.* EGFP$_{retro}$ rats.

was smaller than that achieved by photostimulation of the RVLM (Experiment 1). Moreover, MAP increased in response to 2 min photostimulation of the RVLM, but not of the PVN. While photostimulation of the RVLM is considered to selectively stimulate axons of PVN-RVLM neurons in ChIEF-tdTomato rats, photostimulation of the PVN likely excited neurons whose cell bodies were localized in the PVN, including PVN-RVLM neurons and other sympathoexcitaotory and sympathoinhibitory PVN neurons. Nitrergic and GABAergic neurons are distributed in the PVN (Roland & Sawchenko, 1993; Watkins *et al.*

2009). Endogenous production of nitric oxide in the PVN can cause sympathoinhibition, and this effect is mediated by an intermediary GABA system in the PVN (Zhang & Patel, 1998). Our injection of AAV vectors into the PVN likely transduced nitrergic and/or GABAergic neurons as well as glutamatergic neurons therein. Thus, in Experiment 2, stimulation of sympathoinhibitory PVN neurons in addition to PVN-RVLM glutamatergic neurons and other sympathoexcitaotory PVN neurons, such as nucleus of the solitary tract-projecting PVN neurons (Pittman & Franklin, 1985; Geerling *et al.*
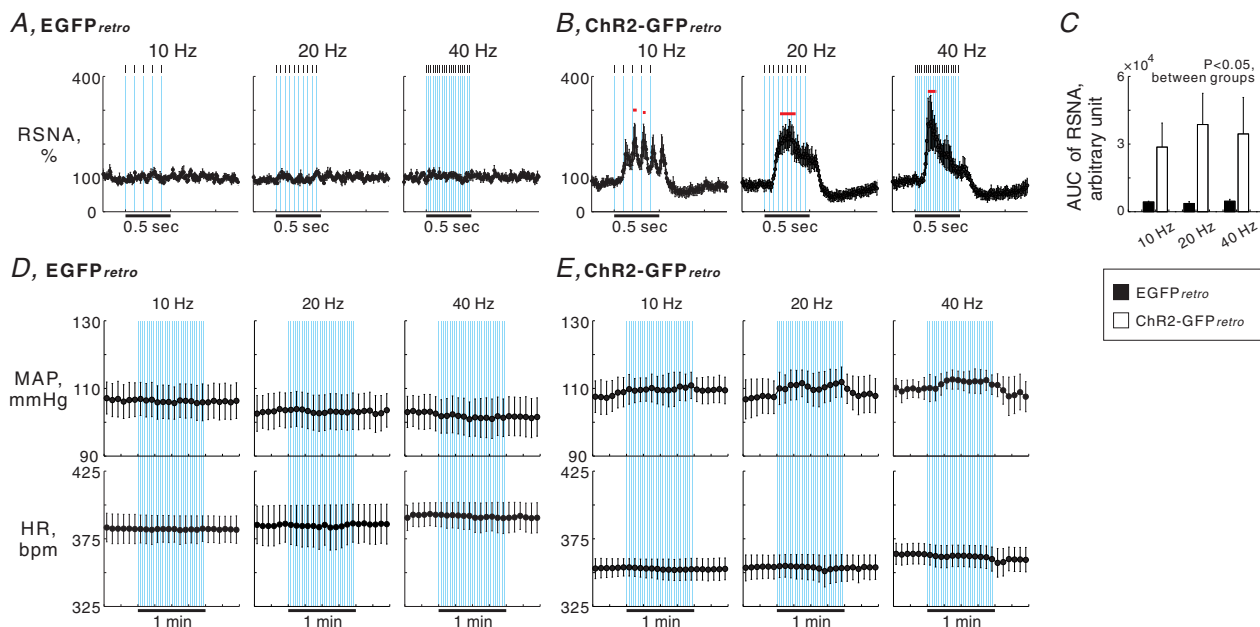
Figure 6. Sympathoexcitation by photostimulation of the cell bodies of PVN-RVLM neurons
A and *B*, 10 ms-averaged time courses of RSNA during a cycle averaged over 30 interventions of photostimulation given to the PVN in 5 EGFP$_{retro}$ (*A*) and 4 ChR2-GFP$_{retro}$ (*B*) rats. Values are means ± SEM. Horizontal red bars, $P < 0.05$ *vs.* baseline. Each blue background represents one photo-pulse given to the PVN, the width of which was 5 ms. *C*, comparisons of RSNA responses to photostimulation (AUC) between the rat groups and among the photostimulation frequencies. *D* and *E*, 5 s-averaged time courses of MAP and HR while 1 min intermittent bouts of photostimulation were given to the PVN in the EGFP$_{retro}$ (*D*) and ChR2-GFP$_{retro}$ (*E*) rats. Each blue background represents one bout of photostimulation given to the PVN, the width of which is 500 ms.

2010), might attenuate sympathoexcitation and pressor responses.

Moreover, the small change in RSNA elicited by photostimulation of the PVN of ChIEF-tdTomato rats might also be attributed to the anaesthetics, urethane and α-chloralose. Stimulation of the rat PVN with low-intensity current or glutamate microinjection decreases RSNA and arterial blood pressure under urethane and α-chloralose anaesthesia (Yamashita *et al.* 1987) but increases those in the conscious state (Kannan *et al.* 1989), suggesting that sympathetic cardiovascular changes in response to stimulation of PVN neuronal cell bodies can be affected by the anaesthetics used. Therefore, urethane and α-chloralose might exert a sympathoinhibitory effect on the sympathetic cardiovascular responses to the optogenetic stimulation of the PVN-RVLM pathway in the present study.

As revealed by superimposing analyses in Experiment 3, when photostimulation was given to the PVN of ChR2-GFP$_{retro}$ rats at 10 Hz with 5 ms pulse duration, each photo-pulse elicited a peak increase in averaged RSNA (Figs. 5*E* and 6*B*). This finding suggests that millisecond-order excitation of PVN-RVLM neurons is capable of increasing the renal sympathetic outflow, although pulse durations shorter than 5 ms were not tested in the present study. No association of each photo-pulse with peak increases in RSNA, when photostimulation was given at either 20 or 40 Hz, may be explained by mixed factors due to higher stimulation frequencies, such as increased temporal summation in the RVLM neurons and/or increased refractory periods of PVN-RVLM neurons following each photo-pulse.

Implications of sympathoexcitatory roles played by PVN-RVLM glutamatergic neurons

While the present study has demonstrated the sympathoexcitatory role of PVN-RVLM glutamatergic neurons, the physiological function of this hypothalamomedullary excitatory pathway in autonomic cardiovascular homeostasis still remains unclear. Nevertheless, dysfunction of this pathway may be associated with aetiologies of cardiovascular diseases. Rodent studies have shown that glutamatergic inputs to the RVLM are exaggerated in animals with heart failure (Wang *et al.* 2009) and hypertension (Bergamaschi *et al.* 1995; Ito *et al.* 2000), thereby leading to sympathetic hyperactivity, a hallmark of these pathological conditions. Experimental evidence also suggests that hyperactivation of PVN neurons contributes to sympathetic hyperactivity in heart failure (Zhang *et al.* 2001, 2002) and hypertension (Allen 2002). Moreover, *in vivo* electrophysiological experiments showed that spontaneous activities of PVN-RVLM neurons in rats with heart failure were increased (Xu *et al.* 2012). Also, whole cell patch-clamp

recordings performed on rat brain slices indicated that in spontaneously hypertensive rats the ionotropic GABA receptor-mediated inhibition of PVN-RVLM neurons is attenuated (Li & Pan, 2006). Based on these findings and the present verification of the sympathoexcitatory role of PVN-RVLM glutamatergic neurons, we hypothesize that in these conditions, hyperactivation of this monosynaptic pathway leads to chronic sympathetic hyperactivity through overactive glutamatergic transmission to RVLM sympathetic premotor neurons. Future studies that test this hypothesis could contribute to our understanding of central circuitry mechanisms underlying the autonomic imbalance associated with cardiovascular diseases.

Activities of PVN-RVLM neurons may contribute to sympathetic adjustments to physical and mental stressors (Dampney, 2015). Previous neural tracing experiments combined with Fos immunohistochemistry revealed that, in rats, 2 days of water deprivation activates PVN-RVLM glutamatergic neurons (Stocker *et al.* 2005, 2006). Moreover, voluntary exercise activates both C1 and non-C1 populations of RVLM neurons as well as PVN neurons (Barna *et al.* 2012; Kumada *et al.* 2017), although the excitation of the PVN-RVLM neurons during exercise has not been verified. It is noted that psychological stresses, such as fear-conditioned stress (Carrive & Gorissen, 2008) and air-puff stress (Furlong *et al.* 2014), activate PVN neurons but not RVLM neurons. This suggests that PVN-RVLM neurons may not be a part of the central circuitries engaged to cope with psychological stressors. Functional contributions of PVN-RVLM glutamatergic neurons to the stress-induced alterations in sympathetic nerve activity should be investigated further in order to understand the central circuit mechanisms of sympathetic adjustments to stressors.

In conclusion, the present study has verified the sympathoexcitatory role of PVN-RVLM glutamatergic neurons. Our results demonstrate that excitation of PVN-RVLM glutamatergic neurons causes sympathoexcitation via, at least in part, stimulation of RVLM C1 neurons. Further studies to determine the involvement of this monosynaptic pathway in chronic sympathetic hyperactivation associated with pathological conditions and acute sympathetic adjustments to stressors will clarify how important this monosynaptic pathway is for maintaining autonomic cardiovascular homeostasis.

References

Abbott SB, Stornetta RL, Socolovsky CS, West GH & Guyenet PG (2009). Photostimulation of channelrhodopsin-2 expressing ventrolateral medullary neurons increases sympathetic nerve activity and blood pressure in rats. *J Physiol* **587**, 5613–5631.

Allen AM (2002). Inhibition of the hypothalamic paraventricular nucleus in spontaneously hypertensive rats

dramatically reduces sympathetic vasomotor tone. *Hypertension* **39**, 275–280.

Barna BF, Takakura AC & Moreira TS (2012). Pontomedullary and hypothalamic distribution of Fos-like immunoreactive neurons after acute exercise in rats. *Neuroscience* **212**, 120–130.

Bergamaschi C, Campos RR, Schor N & Lopes OU (1995). Role of the rostral ventrolateral medulla in maintenance of blood pressure in rats with Goldblatt hypertension. *Hypertension* **26**, 1117–1120.

Brailoiu GC, Dun SL & Dun NJ (2002). Glutamate receptor subunit immunoreactivity in neurons of the rat rostral ventrolateral medulla. *Auton Neurosci Basic Clin* **98**, 55–58.

Carrive P & Gorissen M (2008). Premotor sympathetic neurons of conditioned fear in the rat. *Eur J Neurosci* **28**, 428–446.

Chen QH & Toney GM (2010). In vivo discharge properties of hypothalamic paraventricular nucleus neurons with axonal projections to the rostral ventrolateral medulla. *J Neurophysiol* **103**, 4–15.

Cunningham ET Jr, Bohn MC & Sawchenko PE (1990). Organization of adrenergic inputs to the paraventricular and supraoptic nuclei of the hypothalamus in the rat. *J Comp Neurol* **292**, 651–667.

Dampney RA (2015). Central mechanisms regulating coordinated cardiovascular and respiratory function during stress and arousal. *Am J Physiol Regul Integr Comp Physiol* **309**, R429–R443.

Furlong TM, McDowall LM, Horiuchi J, Polson JW & Dampney RA (2014). The effect of air puff stress on c-Fos expression in rat hypothalamus and brainstem: central circuitry mediating sympathoexcitation and baroreflex resetting. *Eur J Neurosci* **39**, 1429–1438.

Geerling JC, Shin JW, Chimenti PC & Loewy AD (2010). Paraventricular hypothalamic nucleus: axonal projections to the brainstem. *J Comp Neurol* **518**, 1460–1499.

Grundy D (2015). Principles and standards for reporting animal experiments in *The Journal of Physiology* and *Experimental Physiology*. *J Physiol* **593**, 2547–2549.

Guyenet PG (2006). The sympathetic control of blood pressure. *Nat Rev Neurosci* **7**, 335–346.

Häbler HJ, Jänig W & Michaelis M (1994). Respiratory modulation in the activity of sympathetic neurones. *Prog Neurobiol* **43**, 567–606.

Ito S, Komatsu K, Tsukamoto K & Sved AF (2000). Excitatory amino acids in the rostral ventrolateral medulla support blood pressure in spontaneously hypertensive rats. *Hypertension* **35**, 413–417.

Jansen AS, Nguyen XV, Karpitskiy V, Mettenleiter TC & Loewy AD (1995). Central command neurons of the sympathetic nervous system: basis of the fight-or-flight response. *Science* **270**, 644–646.

Kannan H, Hayashida Y & Yamashita H (1989). Increase in sympathetic outflow by paraventricular nucleus stimulation in awake rats. *Am J Physiol Regul Integr Comp Physiol* **256**, R1325–R1330.

Kataoka N, Hioki H, Kaneko T & Nakamura K (2014). Psychological stress activates a dorsomedial hypothalamus-medullary raphe circuit driving brown

adipose tissue thermogenesis and hyperthermia. *Cell Metab* **20**, 346–358.

Koba S, Gao Z & Sinoway LI (2009). Oxidative stress and the muscle reflex in heart failure. *J Physiol* **587**, 5227–5237.

Koba S, Hisatome I & Watanabe T (2014). Central command dysfunction in rats with heart failure is mediated by brain oxidative stress and normalized by exercise training. *J Physiol* **592**, 3917–3931.

Kumada N, Koba S, Hanai E & Watanabe T (2017). Distribution of Fos-immunoreactive cells in the ventral part of rat medulla following voluntary treadmill exercise. *Auton Neurosci Basic Clin* **208**, 80–87.

Li DP & Pan HL (2006). Plasticity of GABAergic control of hypothalamic presympathetic neurons in hypertension. *Am J Physiol Heart Circ Physiol* **290**, H1110–H1119.

Luiten PG, ter Horst GJ, Karst H & Steffens AB (1985). The course of paraventricular hypothalamic efferents to autonomic structures in medulla and spinal cord. *Brain Res* **329**, 374–378.

Morrison SF, Milner TA & Reis DJ (1988). Reticulospinal vasomotor neurons of the rat rostral ventrolateral medulla: relationship to sympathetic nerve activity and the C1 adrenergic cell group. *J Neurosci* **8**, 1286–1301.

Nam H & Kerman IA (2016). Distribution of catecholaminergic presympathetic-premotor neurons in the rat lower brainstem. *Neuroscience* **324**, 430–445.

Paxinos G & Watson C (2007). *The Rat Brain in Stereotaxic Coordinates*. 6th edn. Elsevier, Burlington, MA, USA.

Pittman QJ & Franklin LG (1985). Vasopressin antagonist in nucleus tractus solitarius/vagal area reduces pressor and tachycardia responses to paraventricular nucleus stimulation in rats. *Neurosci Lett* **56**, 155–160.

Pyner S & Coote JH (2000). Identification of branching paraventricular neurons of the hypothalamus that project to the rostroventrolateral medulla and spinal cord. *Neuroscience* **100**, 549–556.

Roland BL & Sawchenko PE (1993). Local origins of some GABAergic projections to the paraventricular and supraoptic nuclei of the hypothalamus in the rat. *J Comp Neurol* **332**, 123–143.

Saper CB, Loewy AD, Swanson LW & Cowan WM (1976). Direct hypothalamo-autonomic connections. *Brain Res* **117**, 305–312.

Schreihofer AM, Stornetta RL & Guyenet PG (2000). Regulation of sympathetic tone and arterial pressure by rostral ventrolateral medulla after depletion of C1 cells in rat. *J Physiol* **529**, 221–236.

Shafton AD, Ryan A & Badoer E (1998). Neurons in the hypothalamic paraventricular nucleus send collaterals to the spinal cord and to the rostral ventrolateral medulla in the rat. *Brain Res* **801**, 239–243.

Stocker SD, Hunwick KJ & Toney GM (2005). Hypothalamic paraventricular nucleus differentially supports lumbar and renal sympathetic outflow in water-deprived rats. *J Physiol* **563**, 249–263.

Stocker SD, Simmons JR, Stornetta RL, Toney GM & Guyenet PG (2006). Water deprivation activates a glutamatergic

projection from the hypothalamic paraventricular nucleus to the rostral ventrolateral medulla. *J Comp Neurol* **494**, 673–685.

Stornetta RL, Sevigny CP, Schreihofer AM, Rosin DL & Guyenet PG (2002). Vesicular glutamate transporter DNPI/VGLUT2 is expressed by both C1 adrenergic and nonaminergic presympathetic vasomotor neurons of the rat medulla. *J Comp Neurol* **444**, 207–220.

Tervo DG, Hwang BY, Viswanathan S, Gaj T, Lavzin M, Ritola KD, Lindo S, Michael S, Kuleshova E, Ojala D, Huang CC, Gerfen CR, Schiller J, Dudman JT, Hantman AW, Looger LL, Schaffer DV & Karpova AY (2016). A designer AAV variant permits efficient retrograde access to projection neurons. *Neuron* **92**, 372–382.

Wang WZ, Gao L, Wang HJ, Zucker IH & Wang W (2009). Tonic glutamatergic input in the rostral ventrolateral medulla is increased in rats with chronic heart failure. *Hypertension* **53**, 370–374.

Watkins ND, Cork SC & Pyner S (2009). An immunohistochemical investigation of the relationship between neuronal nitric oxide synthase, GABA and presympathetic paraventricular neurons in the hypothalamus. *Neuroscience* **159**, 1079–1088.

Xu B, Zheng H & Patel KP (2012). Enhanced activation of RVLM-projecting PVN neurons in rats with chronic heart failure. *Am J Physiol Heart Circ Physiol* **302**, H1700–H1711.

Yamashita H, Kannan H, Kasai M & Osaka T (1987). Decrease in blood pressure by stimulation of the rat hypothalamic paraventricular nucleus with L-glutamate or weak current. *J Auton Nerv Syst* **19**, 229–234.

Yang Z & Coote JH (1998). Influence of the hypothalamic paraventricular nucleus on cardiovascular neurones in the rostral ventrolateral medulla of the rat. *J Physiol* **513**, 521–530.

Yizhar O, Fenno LE, Davidson TJ, Mogri M & Deisseroth K (2011). Optogenetics in neural systems. *Neuron* **71**, 9–34.

Zhang K, Li YF & Patel KP (2001). Blunted nitric oxide-mediated inhibition of renal nerve discharge within PVN of rats with heart failure. *Am J Physiol Heart Circ Physiol* **281**, H995–H1004.

Zhang K & Patel KP (1998). Effect of nitric oxide within the paraventricular nucleus on renal sympathetic nerve discharge: role of GABA. *Am J Physiol Regul Integr Comp Physiol* **275**, R728–R734.

Zhang ZH, Francis J, Weiss RM & Felder RB (2002). The renin-angiotensin-aldosterone system excites hypothalamic paraventricular nucleus neurons in heart failure. *Am J Physiol Heart Circ Physiol* **283**, H423–H433.

Zingg B, Chou XL, Zhang ZG, Mesik L, Liang F, Tao HW & Zhang LI (2017). AAV-mediated anterograde transsynaptic tagging: mapping corticocollicular input-defined neural pathways for defense behaviors. *Neuron* **93**, 33–47.

Additional information

Competing interests

None declared.

Author contributions

All experiments, besides preparations of AAV2/1-CMV-ChIEF-tdTomato and AAV2/1-CMV-palGFP, were performed at the Division of Integrative Physiology, Tottori University Faculty of Medicine. Preparations of the AAVs were conducted at the Department of Integrative Physiology, Nagoya University Graduate School of Medicine. S.K.: conception and design of the work, provision of study materials, assembly of data; data analysis and interpretation; manuscript drafting, editing and revising. E.H.: assembly of data; data analysis and interpretation. N.Ku.: assembly of data; data analysis and interpretation. N.Ka.: provision of study materials. K.N.: provision of study materials; data interpretation; manuscript editing and revising critically for important intellectual content. T.W.: provision of study materials. All authors approved the final version of the manuscript, agree to be accountable for all aspects of the work in ensuring that questions related to the accuracy or integrity of any part of the work are appropriately investigated and resolved, and qualified for authorship. All those who qualify for authorship are listed.